Japanese Journal of Applied Physics **51** (2012) 05EA02 **REGULAR PAPER**
DOI: 10.1143/JJAP.51.05EA02

In-situ Spectroscopic Ellipsometry of the Cu Deposition Process from Supercritical Fluids: Evidence of an Abnormal Surface Layer Formation

Takuya Sasaki, Yukihiro Tamegai, Takahiro Ueno, Mitsuhiro Watanabe, Lianhua Jin, and Eiichi Kondoh*

Graduate School of Medicine and Engineering, University of Yamanashi, Kofu 400-8511, Japan

Received October 14, 2011; accepted January 17, 2012; published online May 21, 2012

In this paper, we report *in-situ* spectroscopic ellipsometry of Cu deposition from supercritical carbon dioxide fluids. The motivations of this work were 1) to perform a detailed observation of Cu growth with precision optical metrology, 2) to study substrate dependence on Cu growth, particularly for Ru and TiN substrates in the present case, and 3) to demonstrate the possibility and usefulness of ellipsometry for diagnosing supercritical fluid processing. The Cu deposition was carried out through hydrogen reduction of a Cu β-diketonate precursor at 160–180 °C. During growth, a very large deviation of ellipsometric parameters (Ψ and Δ) from a single-layer model prediction was observed; this deviation was much larger than that expected from island formation which has been frequently reported in *in-situ* ellipsometric observation of the vapor growth of thin films. From model analyses, it was found that an abnormal dielectric layer having a high refractive index and a thickness of 10–50 nm is present on the growing Cu surface. The refractive index of this layer was (1.5–2) + (0.2–0.3)*i*; and from this, we concluded that this layer is the condensed precursor. The condensed layer develops prior to Cu nucleation. As for the substrate dependence on Cu growth, both layers develop faster on Ru than on TiN. This corresponds to the fact that chemisorption occurs more easily on Ru. The deposition kinetics under the presence of the condensed layer are also discussed.

1. Introduction

The dimensions of LSI interconnects are continuously being downscaled. Existing deposition techniques such as physical vapor deposition (PVD), chemical vapor deposition (CVD), and electroplating may face limitations for fabricating nm-sized interconnects. Novel interconnect fabrication technologies are always in demand to follow miniaturization.

Thin film deposition in supercritical CO_2 ($scCO_2$) fluids has been proposed as an alternative technology. $ScCO_2$ is a fluid that exists above the critical point of CO_2 (7.38 MPa and 31.1 °C[1]). It has zero surface tension, low viscosity and good diffusivity like a gas, and high density and solvent capability like a liquid. In addition to these, CO_2 is inert and harmless to humans, inexpensive, and recyclable.

Metal deposition in $scCO_2$ has been reported for Cu,[2–4] Ni,[3] Pd,[3,5,6] Pt,[5,7] Rh,[5] Ru,[8,9] Au,[5] and Ag.[10,11] In this technique, a precursor, usually an organometal compound, is dissolved in $scCO_2$, together with hydrogen or another reducing agent[11] if necessary, so that metal is deposited through thermal reaction. An example of chemical formulation of this reaction is $ML_2 + H_2 \rightarrow M + HL$, where M refers to metal and L is a ligand. The excellent capability of this technique is for filling narrow features, such as nanpores,[11–14] trenches,[3,4,15] and via holes[15,16] with a metal has been demonstrated successfully, which promises the application of this technique to fabricating small interconnects.

The great importance of *in-situ* diagnostics is well recognized for understanding the deposition mechanism of thin film processes. In this paper, we studied *in-situ* spectroscopic ellipsometry on Cu growth in $scCO_2$ using two different substrates. The motivations of this work were three-fold.

Firstly, the growth manner of Cu was found to have a surface dependency. We studied the initial growth and morphology development of Cu deposition previously.[17] Cu grown on Cu-seed had a rough granular structure but showed a bottom-up growth manner in narrow trenches. Contrarily, on Ru-liner, we observed a smooth and conformal growth behavior. As understood, the initial growth greatly influences the overall growth mode, which is obviously a crucial subject to study in metallization.

Secondary, contrary to PVD or CVD, a very limited number of studies have been carried out on *in-situ* diagnostics of thin film processes in supercritical fluids. In order to highlight this, we here briefly state the current status of *in-situ* diagnostics work related to material synthesis in supercritical solutions.

Adsorption spectroscopy and chromatography are popular techniques as *in-situ* diagnostics of chemical reactions in supercritical fluid processing. Thermal decomposition of metal chelates has been studied with visible and UV adsorption spectroscopy,[18,19] but this is not a direct observation of precipitation or deposition processes. Optical and X-ray scattering techniques have been applied to observe particle synthesis,[20,21] but these techniques are not very useful for the investigation of thin film processes. Quartz crystal microbalance (QCM) is a very useful *in-situ* tool for measuring the changes of thin films. In the QCM technique, the sample is directly formed on the membrane of a QCM, and therefore the use of a desired substrate is not possible. Moreover, the measurement environment is limited so as to enable the QCM, for instance, the monitoring at elevated temperatures is not possible.

Recently, Momose *et al.* reported *in-situ* measurement of the spectroscopic reflectance for Cu thin film growth in an $scCO_2$–H_2–CuL_2 solution.[22] They studied the evolution of thin films structure from isolated islands to a continuous film by observing the change in spectrum of the reflected light or from colors of the surface. However, physical information and its meanings obtainable from this method are very limited.

Ellipsometry is a versatile technique for determining optical properties of surfaces and thin films from the polarization of reflected light. It is a non-contact, non-destructive and fast technique, and is applicable to any flat substrate processed at elevated temperatures in an optically transparent environment. In addition, ellipsometry can determine physical structures such as film stacking, film thicknesses and dielectric functions very accurately. Only a few papers have been published so far on the ellipsometry of

*E-mail address: kondoh@yamanashi.ac.jp

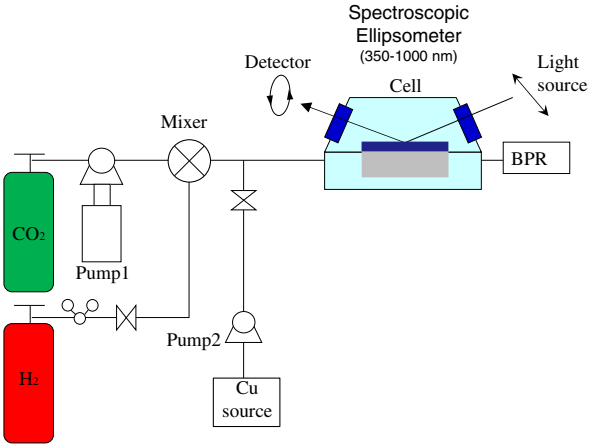

Fig. 1. (Color online) Experimental apparatus.

Table I. Experimental conditions.

Substrates	$Si/SiO_2/TiN$, $Si/SiO_2/Ru$
$Cu(dibm)_2$ concentration (%)	4.6×10^{-3}
Acetone concentration (%)	5.0
Hydrogen concentration (%)	1.45
Total pressure (MPa)	10
Temperature (°C)	160, 180, 200
Deposition time (min)	60

electronic materials in $scCO_2$.[23,24] Therefore, *in-situ* ellipsometric observation itself is a challenging research topic in terms of metrology in $scCO_2$ engineering, especially in the field of microelectronics.

2. Experimental Methods

The experimental apparatus used in this work is shown in Fig. 1. This apparatus was designed to allow for ellipsometric measurements of a specimen placed in a high-pressure optical cell under supplying a Cu precursor at elevated temperatures. The basic configuration of the fluid supply system was mostly identical to the one we reported elsewhere.[25,26] The optical cell is a stainless steel-made high-pressure vessel having two Pyrex™ glass viewports, configured to carry out ellipsometric measurements at an incident angle of 70°. The specimen was placed horizontally in the cell and was heated with a built-in cartridge heater. Samples used were pieces of silicon wafers coated with TiN or Ru. The deposition conditions were a pressure of 10 MPa and temperatures of 160–200 °C. The other conditions are listed in Table I. After reaching the target temperature, only H_2-mixed CO_2 was supplied for system stabilization at first, and then the precursor was supplied for 60 min.

The polarization parameters (Ψ, Δ) — the complex reflectivity ratio of p- and s-polarized lights, and the phase shift between p- and s-polarized lights, respectively — were measured for the wavelength range of 350–1000 nm during the experiments. The calibration procedure of the birefringence effect of the windows is described in the Appendix.

3. Results

In this section, we present the behaviors of ellipsometric parameters during Cu growth (§3.1) and the surface topography of Cu films in the next (§3.2). The presented data are examined and discussed in the subsequent section.

3.1 Time changes of ellipsometric parameters

Metal-colored Cu films were obtained after deposition runs, except for one case stated otherwise. The examples of spectra changes during the precursor supply are shown in Figs. 2 and 3. The Ψ and Δ spectra conformed to the same locations as time passed. The overlapping final spectra are identical to the spectrum of Cu in terms of its profile. In order to highlight the behavior of Ψ and Δ, the values at a wavelength of 633 nm are shown hereafter in this subsection as customary in ellipsometry.

Figures 4 and 5 show the time changes of Ψ and Δ during deposition at 633 nm. Ψ and Δ for a run using TiN started from their values of TiN ($\Psi = 21°$, $\Delta = 66°$) and approached the values of Cu ($\Psi = 42°$, $\Delta = 90°$) when the temperature was as high as 200 °C. (This value set of Cu is not exactly identical to the theoretical value set. The reason is described later.) The deposition using Ru ($\Psi = 37°$, $\Delta = 154°$) showed the same behavior. The times needed to reach the stationary values were different for TiN and Ru, where a longer time of approx. 15 min was need to reach for TiN than the approx. 10 min for Ru.

In Fig. 6, Δ is plotted against Ψ. This Ψ–Δ chart gives a better understanding of the physical meanings of the time changes of Ψ and Δ. When deposited on TiN at 200 °C [Fig. 6(a)], the Ψ–Δ trajectory starts from the point of the TiN substrate and ends at $(\Psi, \Delta) = (42°, 90°)$. On Ru substrates, the trajectories start from the point of Ru, travel roughly downwards, and end at around $(\Psi, \Delta) = (42°, 90°)$ [Fig. 6(b)].

3.2 Cu surfaces after deposition

Ex-situ spectroscopic ellipsometry measurements were carried out on the specimens in the atmosphere after deposition, and the (Ψ, Δ) coordinate points of these specimens are also plotted in Fig. 6.

Surface roughness can influence the ellipsometric parameters of the films, and therefore, surface probe microscope (SPM) images were obtained for the Cu surfaces after deposition at 200 °C (Fig. 7). The arithmetic mean roughness (R_a) of the surface of Cu deposited on TiN at 200 °C was 0.41 nm, and R_a of Cu on Ru was 0.99 nm.

4. Discussion

4.1 Surface and film structures

4.1.1 Effect of surface roughness or island formation

The behaviors of the trajectories shown in Fig. 6 are quite unusual. The dashed lines in Fig. 6 are theoretical trajectories obtained under the assumption of a thickening of a continuous single Cu layer on the substrate. In those models, the refractive index of Cu was set to $0.23 + 3.42i$,[27] and the refractive indices of the substrates were calculated from the actual ellipsometry measurements. The curves start from the points of the substrates and reach the theoretical point of Cu, $(\Psi, \Delta) = (41.6°, 89.6°)$, where the experimental

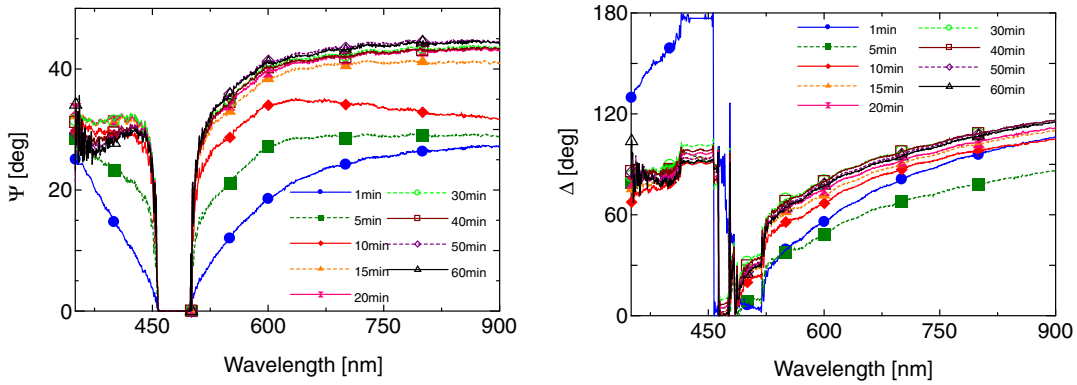

Fig. 2. (Color online) Ψ and Δ spectra taken at 1, 5, 10, 15, 20, 30, 40, 50, 60 min using a TiN substrate at 200 °C.

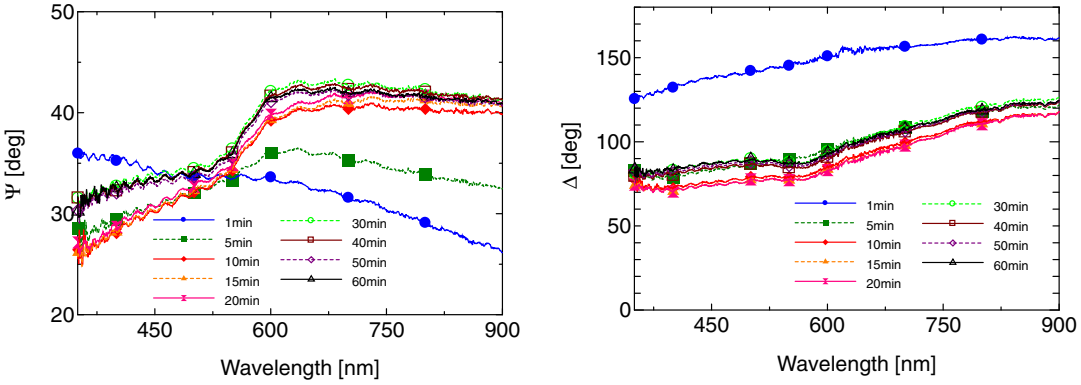

Fig. 3. (Color online) Ψ and Δ spectra taken at 1, 5, 10, 15, 20, 30, 40, 50, 60 min using a Ru substrate at 200 °C.

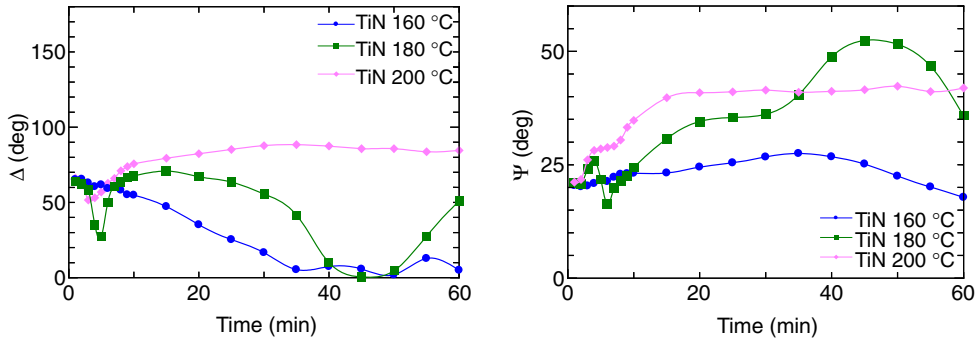

Fig. 4. (Color online) Time changes of Ψ and Δ for TiN substrate.

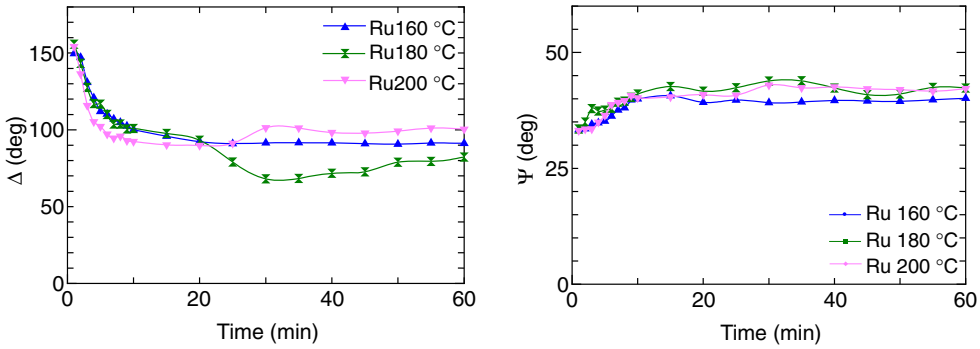

Fig. 5. (Color online) Time changes of Ψ and Δ for Ru substrate.

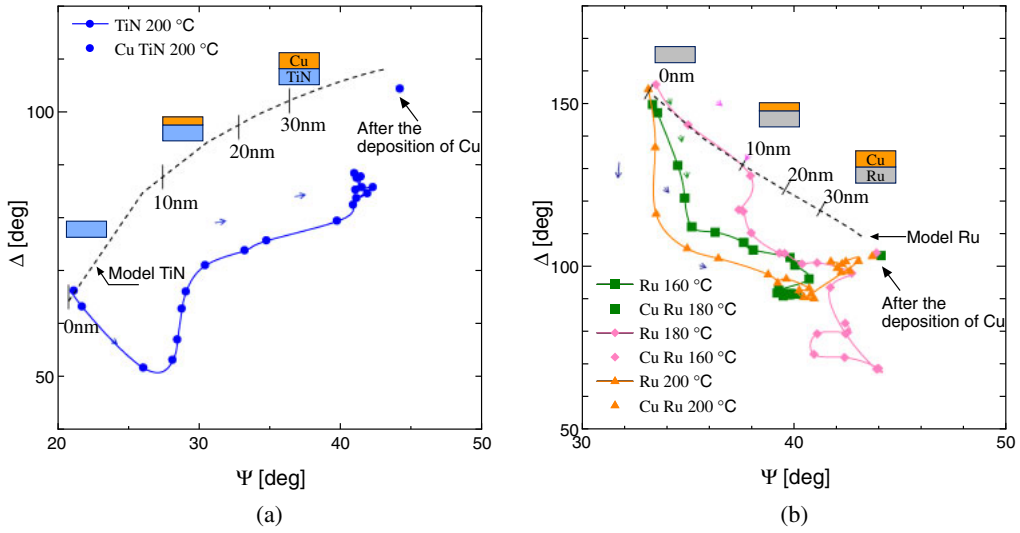

Fig. 6. (Color online) Ψ versus Δ plots of experimental data (connected symbols) with theoretical trajectories (dashed lines) for Ru substrates (a) and TiN substrate (b). For details, see §4.1.1.

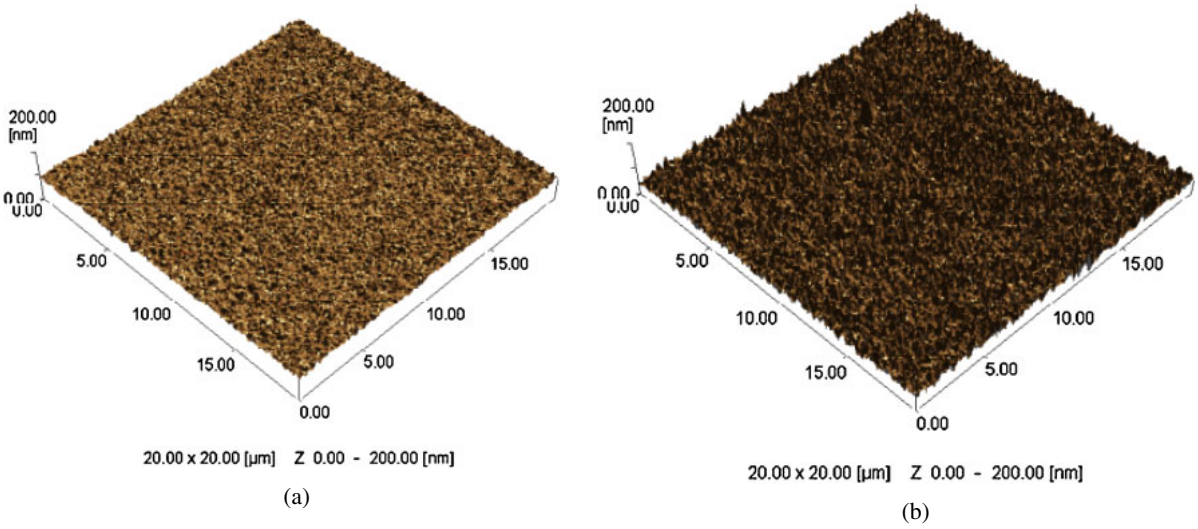

Fig. 7. (Color online) SPM images of Cu surfaces taken after deposition in the atmosphere. (a) Substrate, TiN; deposition temperature, 200 °C; $R_a = 0.41$ nm. (b) Substrate, Ru; deposition temperature, 200 °C; $R_a = 0.99$ nm.

trajectories are very much deviated from these theoretical curves.

A discontinuous film structure has a lower optical thickness than a continuous film, and thus the film discontinuity can result in a deviation of ellipsometric parameters from a continuous model. It is known that the thin film growth process starts with nucleation on a substrate, and after the evolution of the nuclei to islands, the islands coalesced, and finally, a continuous film is formed. Such a deviation of ellipsometric parameters from a continuous model can be observed at an early stage of film growth. In fact, many investigations have been made using this principle to study the initial film growth in a vacuum.[28,29)]

However, in the present case, the formation of a discontinuous structure is not the main reason. For qualitative confirmation, let us assume a growing Cu surface has a 1-nm-thick island/rough structure consisting of 50% Cu–50% void. (This thickness is adopted from an R_a value shown in §3.2.) When this layer is present on the TiN substrate, a model calculation gives theoretical ellipsometric parameters of $(\Psi, \Delta) = (21.7°, 67.0°)$. These value set is very close to those of a 1-nm-thick *continuous* Cu film of $(\Psi, \Delta) = (21.2°, 71.4°)$. Similarly, bulk Cu having a 1-nm-thick film consisting of 50% Cu–50% void on top has parameters of $(\Psi, \Delta) = (42.9°, 106.4°)$, close to those of bulk Cu itself, $(\Psi, \Delta) = (43.3°, 108.0°)$.[30)] The Ψ and Δ obtained after deposition were close to the theoretical values of Cu; the differences were 0.7° for Ψ and 4.6° for Δ. Although these differences are not negligible in terms of high accuracy of ellipsometry, they are obviously much smaller than the differences observed during growth.

Therefore, we can safely say that the surface roughness or island growth did not affect the measurements. This means that a certain abnormal optical behavior occurred only in

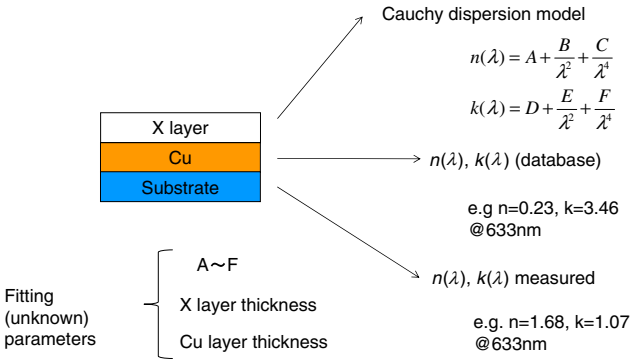

Fig. 8. (Color online) Optical model structure used in analysis.

supercritical solutions. We concluded that an unknown layer is present on the growing Cu layer during deposition in $scCO_2$, and this will be discussed next.

4.1.2 Optical structure of an abnormal layer

The model used for analysis of the abnormal layer, named X layer hereafter, is shown in Fig. 8. The model structure is a stacked layer consisting of the top X layer, a continuous Cu layer underneath, and the substrate. The X layer was modeled as an absorbing Cauchy layer, of which dispersion of the real and imaginary parts of the refractive index, $n(\lambda)$ and $k(\lambda)$, respectively, are expressed as functions of a wavelength, λ.[31)]

$$n(\lambda) = A + \frac{B}{\lambda^2} + \frac{C}{\lambda^4}, \quad (1)$$

$$k(\lambda) = D + \frac{E}{\lambda^2} + \frac{F}{\lambda^4}, \quad (2)$$

where A–F are constants. The thicknesses of Cu and the X layer were set as unknown parameters, and therefore the total number of unknown parameter is eight. From this model and the acquired spectra of Ψ and Δ, these eight parameters were obtained for all spectra taken during each run using a non-liner fitting method using built-in software of the ellipsometer. Figures 9 and 10 show an example the results of numerical fitting which show very good agreement between the experimental and fitted spectra.

All the A–F parameters between 30 and 60 min were averaged. The reason for this treatment is as follows. One of our major interests is in the initial growth of Cu. The nucleating thin films can have various structures in terms of topography, discontinuity, and island density, and the complex reflectivity of the surface is highly dependent of such surface structures. Therefore, precise determination of the optical properties of the X layer is very difficult. The situation becomes easier when the Cu becomes thick. The complex reflectivity of a thick Cu film is independent of the film thickness and the substrate material due to a large extinction coefficient or a small skin depth of Cu. If the Cu film is thick enough, the number of unknown parameters decreases. Minding that the time needed to reach stationary Ψ and Δ values (see Figs. 4 and 5) as well as the observed deposition rates, we assumed that 30 min is long enough to allow for this thick Cu approximation, except for a run carried out using TiN and at 160 °C. Table II shows raw data of the time changes of thickness, n, and k (633 nm) of the X layer determined by model fitting. Obviously, the spread of the refractive index is small after 30 min, supporting our averaging treatment.

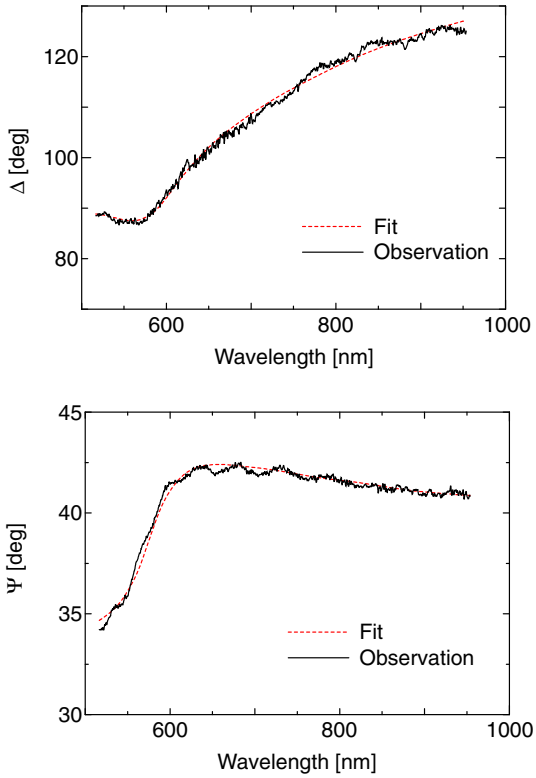

Fig. 9. (Color online) Results of fitting Ψ and Δ spectra. Substrate, TiN; deposition temperature, 200 °C; time, 25 min.

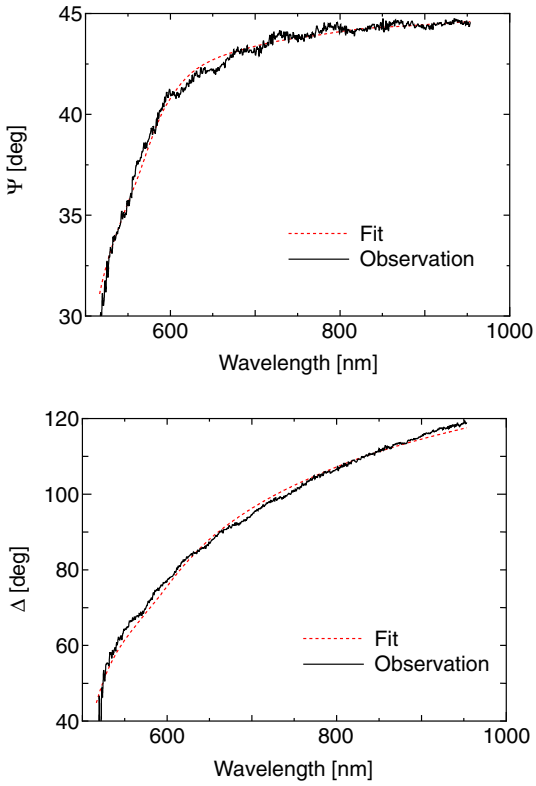

Fig. 10. (Color online) Results of fitting Ψ and Δ spectra. Substrate, Ru; deposition temperature, 200 °C; time 25 min.

Table II. Examples of time changes of X layer thickness, n and k of X layer on TiN and Ru substrates at 200 °C. The X layer thicknesses are not exactly the same as those in Figs. 11 and 12 (see text).

Time (min)	TiN 200 °C			Ru 200 °C		
	X layer thickness (nm)	n	k	X layer thickness (nm)	n	k
20	18	2.00	0.38	14	1.95	0.43
25	14	2.09	0.38	12	1.98	0.51
30	12	2.15	0.35	8	1.46	0.08
35	13	2.08	0.43	10	1.33	0.11
40	14	2.00	0.38	8	1.70	0.20
45	16	1.96	0.25	9	1.67	0.25
50	17	1.91	0.14	10	1.44	0.22
55	18	1.98	0.3	11	1.29	0.20
60	17	1.96	0.19	11	1.33	0.14

Table III. Comparison of n and k at a wavelength of 633 nm.

Material	n	k	X layer thickness (nm)
X layer on Cu/TiN	2.00	0.29	15–40
X layer on Cu/Ru	1.46	0.17	15–50
Cu	0.25	3.41	—
CuO	2.69	0.43	
Cu_2O	2.93	0.11	—

At the end of this subsection, the obtained refractive indices at 633 nm are summarized in Table III. The X layer has a large n value and nonzero small k value. That is, the X layer is found to be an absorbing dielectric film.

4.1.3 Development of the X layer

Next, using the $n(\lambda)$ and $k(\lambda)$ obtained above, the thicknesses of Cu and the X layer were determined over all the deposition time range, where in this case, only two parameters were set as unknown in the model fitting computation.

The results of the analyses are shown in Figs. 11 and 12.[32] The thickness of Cu is not reliable over 20 nm, as the skin depth of Cu is 10–20 nm in the wavelength range used. As has been seen, the X layer begins to develop immediately after starting the precursor supply (0–5 min) and grow continuously, except when the temperature is high (200 °C). The stationary thickness is 15–20 nm (see Table II). The Cu layer grows after an increase in the X layer thickness. Comparing Ru substrate (Fig. 11) and TiN substrate (Fig. 12) at a low temperature, it can be seen that Cu starts to grow at a deposition time of a few minutes, much faster on the Ru layer. On the contrary, the X layer does not grow earlier on the TiN, and Cu starts to grow at about 15 min, later than on Ru. At a higher temperature, the growth start time of Cu is reduced, but the trend is the same.

4.2 Cu deposition mechanism

4.2.1 Identification of the X layer

As shown above, the X layer has a large refractive index (real part), which indicates that strong polarization occurs by the electric field of light. Among substances present in our system [CO_2, Cu, acetone, Cu(dibm)$_2$], only Cu(dibm)$_2$ is expected to exhibit such a high refractive index.

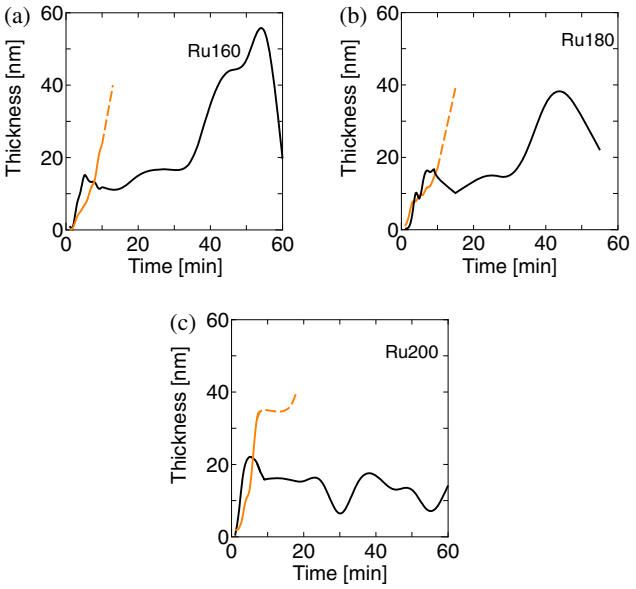

Fig. 11. (Color online) Time changes of the thicknesses of the Cu and X layers on Ru at temperatures of 160 (a), 180 (b), and 200 °C (c).

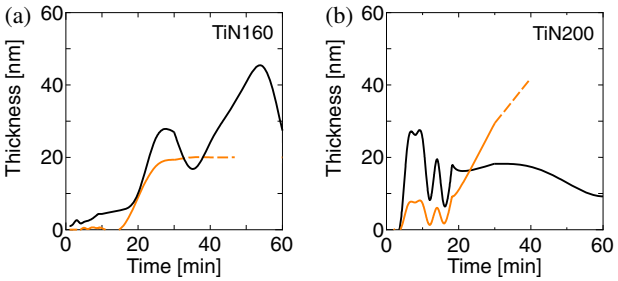

Fig. 12. (Color online) Time changes of the thicknesses of the Cu and X layers on TiN at temperatures of 160 (a) and 200 °C (b).

The refractive index of Cu^{II}(dibm)$_2$ or related compounds is not currently available to the authors.[33] $Cu^{II}L_2$ — here L is a β-diketonate ligand — complexes have a divalent copper ion in the center of the molecule. The optical properties of the visible range of these compounds are dominated by this optically active ion. On this basis, the refractive indices of Cu,[27] CuO,[27] (divalent) and Cu_2O[27] (monovalent) are shown in Table III for comparison. Either the real or imaginary parts of the refractive indices of the X layer are slightly smaller than those of CuO or Cu_2O, and are very different from Cu. This indicates that the X layer has a lower polarization density than the others, which fairly agrees with our general sense evoked by minding the structure of $Cu^{II}L_2$. Indeed, a Cu complex having a similar arrangement of oxygen atoms has a refractive index of about $1.9 + 0.07i$,[34] which is close to our observation.

Therefore, we conclude that the X layer is a thick condensed layer of Cu(dibm)$_2$, or at least its derivative or an intermediate formed in the course of the Cu deposition reaction[35] (Fig. 13). The following discussion is made on this basis.

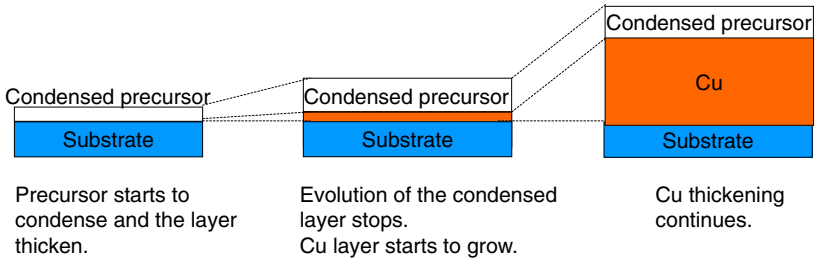

Fig. 13. (Color online) Model of the development of the Cu and X layers during Cu deposition.

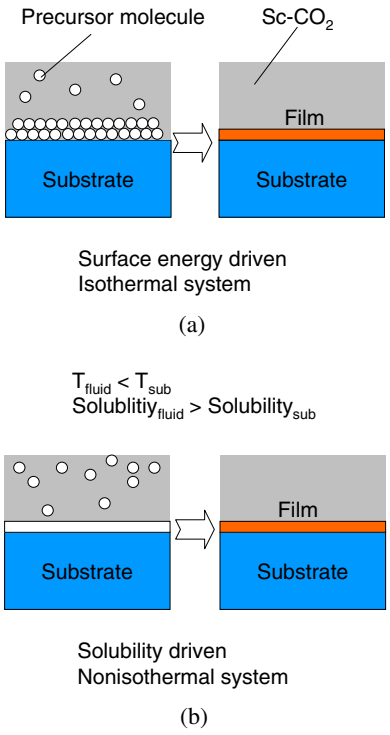

Fig. 14. (Color online) (a) Multilayer adsorption model (refs. 37 and 38) and (b) supersaturation model (ref. 39) proposed on the formation of the condensed precursor layer during thin film deposition in $scCO_2$.

4.2.2 Mechanism of X layer formation

It has been pointed out that a metal complex precursor can condense at the surface or substrates during film growth from $scCO_2$.

Kondoh *et al.* advocated multiplayer adsorption or liquefaction of the precursor from their observation of *topography sensitive* growth as a phenomenon where metal growth occurs selectively in concave features.[36–38] They used a hot-wall batch reactor and therefore assumed a thermodynamically isothermal system where the multilayer adsorption occurs by attractive interactions between precursor molecules or physisorption [see Fig. 14(a)].

In their different experiments using a flow-type reactor, they also showed that the deposition rate follows a Brunauer–Emmett–Teller (BET) type multilayer adsorption isotherm, especially at higher temperatures of 240–280 °C. The reactor was designed as a slit-like hot-wall reactor where the temperature of the inflowing fluid increases quickly, and therefore the system is assumed to be isothermal, though it was not particularly mentioned.

Figures 11 and 12 show that a thicker layer of the condensed precursor is formed on Ru earlier. As physisorption occurs on the already adsorbed layers, this indicates that chemisorption of the precursor occurs better on Ru, which has higher reactivity than TiN. In terms of the temperature dependence of the condensation, the adsorption enthalpy of $Cu(dibm)_2$ is likely to be positive, and therefore $Cu(dibm)_2$ may adsorb less as the temperature increases.[25] Figures 11 and 12 show the thickness of the X layer seems to have a negative dependence on temperature, which seems in good agreement with the above mentioned results.

Uchida *et al.* pointed out in their study of TiO_2 thin film growth that a precursor of $Ti(O(CH_3)_2)_2(dpm)_2$ (dpm: dipivaloylmethanate) is supersaturated at the substrate surface and condenses as a liquid state.[39] Their apparatus was intentionally arranged to make a large temperature difference between the supplied fluid (low temperature, e.g., 40 °C) and the substrate (high temperature, e.g., 100 °C). Solubility of a substance in $scCO_2$ depends both on the density of the fluid and on the vapor pressure of the substance. An increase in temperature decreases the fluid density (the density of $scCO_2$ changes as functions of temperature and pressure), and thus the solubility decreases, but at the same time, the solubility increases because the vapor pressure increases. Which is dominant depends on the temperature range, and the solubility minimum will appear at a particular temperature (Chrastil's law[40]). Uchida postulated that the fluid temperature increased and the solubility of the precursor decreased during the travel of the fluid, and the condensation of the precursor takes place at the surface due to the supersaturation [see Fig. 14(b)].

Can such a temperature difference function as a driving force to the precursor condensation also in the present work? To answer this, the temperature dependence of the solubility of $Cu(dpm)_2$ and the temperature distribution in our optical cell should be discussed.

Few studies have reported on the solubility of metal complexes in $scCO_2$ at elevated temperatures.[41] Recently, Haruki *et al.*[42] studied the temperature dependences of the solubility of metal β-diketonate complexes [$Cu(dibm)_2$ is a family compound]. They reported that the solubility minimum point appears at about 100 °C, and above this temperature the solubility increases with temperature. Unfortunately, their measurements were not conducted at temperatures as high as our deposition temperatures (160–200 °C), presumably due to experimental difficulty. However, Chrastil's law safely forecasts the solubility of $Cu(dibm)_2$ increases with temperature in our temperature range,[43] as far as its significant decomposition does not occur.

As for the temperature distribution, from computational fluid dynamic work on our cell, the temperature of the fluid adjacent of the substrate was found to be several degrees lower than the substrate. In conclusion, it is still not very clear that such a temperature difference can make a temperature differential condensation; however, we cannot exclude its possibility.

In this subsection, multilayer adsorption and solubility differential condensation are discussed as possible mechanisms of the formation of the X layer. In general, when the temperature difference is small, multiplayer adsorption will occur preferentially, whereas the solubility differential mechanism will be dominant when the temperature difference is large. In either case, condensed molecules physically adsorb on already adsorbed molecules; in this sense there is no difference in between. In an actual case, the X layer contains different substances (such as CO_2 and acetone) and chemical reactions may occur in the layer. Therefore, the detailed mechanism will be greatly complicated.

4.2.3 X layer and deposition kinetics

Mechanisms of low temperature CVD have been well established on the basis of catalysis chemistry, where monoadsorbed species react at the surface so as to form nonvolatile species. Cu deposition in $scCO_2$ has been illustrated likewise.[44,45] The basic formula for deposition reaction of our system is $CuL_2 + H_2 \rightarrow Cu + 2HL$; and if we follow the scheme of Cu CVD,[46–48] dissociatively (mono)adsorbed CuL_2 and H_2 will react together on the growing surface (Langmuir–Hinshelwood model).

Even when the surface condensation occurs, the molecules at the surface can chemically adsorb. In this case, the coverage of the chemisorbed precursor is to be very large because the molecular density of the precursor is extremely high adjacent to the substrate. This condition can be treated as a special case of the Langmuir–Hinshelwood model, and as far as we adhere to this scheme, we basically do not need to modify the surface reaction mechanism itself.

However, we believe that this model needs to be modified when the condensation of the precursor occurs. H_2 will diffuse through the thick condensed layer and can react with the precursor molecules. In this case, two possible features should be noticed. Firstly, the deposition reaction can proceed in a homogenous manner so that the reaction takes place anywhere in the layer, especially at higher temperatures. This is identical to that the reaction kinetics do not follow the monoadsorption (Langmuir-type) model, but follow condensation or multilayer adsorption kinetics. Indeed, it was shown that the Cu growth kinetics in $scCO_2$ follow the BET type multilayer adsorption at high temperatures,[38] as discussed in §4.2.2. Secondary, the reaction can proceed non-dissociatively, at least apparently. Experimental reaction kinetics showed that $Cu(dibm)_2$ does not dissociate, whereas H_2 dissociates in the same system as the present work.[25] This implies the possibility of high rate deposition, as the adsorption amount does not saturate even when increasing the concentration $Cu(dibm)_2$.

The homogeneous reaction manner evokes the belief that preferential formation of particles will occur. However, as understood from the ellipsometric measurements and the SPM topography, the actual deposit obtained did not hold a significant amount of particles. Even if there is a tendency of the particle formation, the deposited granular Cu is thought to be unstable in $scCO_2$, and a continuous thin film is formed because Cu easily aggregates and sinters in $scCO_2$.[17,49]

4.3 Substrate effects on initial growth of Cu

4.3.1 X layer development

Ru is now gaining a lot of attention in LSI metallization. For example, uses as a barrier metal[50–52] and as a seed/liner[53–55] metal have been proposed. It has been reported that Cu nucleates and grows promptly on Ru.[56,57] This is because Ru is a noble metal, does not form a rigid oxide, has good wettability between Cu and Ru, and can play a catalytic role in nucleation.

In the present study, we observed that the acquired Ψ and Δ spectrum conformed to their final forms, which are practically identical to the spectra of Cu, faster on Ru than on TiN (Figs. 2 and 3). The times needed to change to the Cu spectra were approximately 10 min for Ru and 15 min for TiN (Figs. 4 and 5). Taking into account the fact that only a sufficiently thick (10–20 nm) film exhibits the Cu spectrum (see §4.1.2), it is obvious that the nucleation and island formation occurred much earlier than the abovementioned times. We can also see the inertness of TiN from Fig. 12. The Cu growth on Ru did not show significant temperature dependences, whereas on TiN, a long incubation time was observed when the temperature was lowered. This tendency is in good agreement with a previous observation.[22]

Figure 11 also shows that a thicker layer of the condensed precursor is formed on Ru earlier. Physisorption occurs on the already adsorbed layers, and therefore, the earlier formation shows that chemisorption of the precursor occurs better on Ru. This observation is also in agreement with the good reactivity of Ru.

4.3.2 Cu growth

Copper growth rate (*GR*) was obtained from the data used for Figs. 11 and 12 and are listed in Table IV. Arrhenius equations determined are:

$$GR = \begin{cases} 6870 \exp\left(-\dfrac{3580}{T}\right) & \text{nm/min for TiN,} \\ 22000 \exp\left(-\dfrac{4790}{T}\right) & \text{nm/min for Ru,} \end{cases}$$

where T is the absolute temperature in Kelvin. The activation energies are 0.31 and 0.41 eV, which are within the range reported before (refs. 25 and 45). A very interesting fact is that the preexponential factors are quite different from each other; Cu grows almost three times faster on Ru. The preexponential factor is a product of reaction probability and the densities of reaction species. The reaction probability is related to the chemical reaction mechanism, and there is no difference between Cu growth on Ru and on TiN because the same experimental conditions were employed. This difference in growth rate originates from the difference in the X layer.

The thickness is dependent on the temperature, as stated previously (§4.2.2). If the temperature is high, the thickness becomes smaller and the growth rate increases. The X layer thickness increases before Cu film growth. This suggests that the X layer is a source of growing species and agrees with

Table IV. Cu growth rates on TiN and Ru obtained by optical model fitting.

Temperature (°C)	TiN	Ru
160	1.74	3.77
180	—	4.46
200	3.51	9.70

our discussion that the X layer is a condensed precursor layer. On the other hand, the X layer seems to have no dependence on the substrate, which is contradictory to the above discussion. Attention must be paid to the lower refractive index of the X layer present on Cu/Ru. A low refractive index indicates lower precursor molecules are involved in the layer. According to our discussion in §4.2.3, the deposition reaction proceeds in a homogeneous manner in the layer. A lower precursor concentration can be a consequence of fast precursor consumption in the X layer. We presume that this less condensed layer has a lower viscosity and molecules can more easily move, which leads to a higher reaction probability and thus a higher growth rate.

The precursor density in the X layer is thought to be determined at a very early stage of Cu growth. On Ru, since the nucleation proceeds promptly, more molecules are consumed, and the density of the layer becomes the smaller. The continuing Cu deposition occurs with this low density layer, and therefore a higher growth rate and lower density are preserved. Contrarily, on TiN, the X layer builds up during a longer incubation time, and less precursor molecules are consumed when Cu starts to grow. As a result, the density of the X layer does not decrease, and thus the deposition reaction rate becomes smaller.

5. Conclusions

In this study, Cu thin film deposition proceeding in $scCO_2$ was monitored by *in-situ* spectroscopic for the first time.

1) While supplying the precursor, the spectrum changed from the initial spectrum of the substrate to the final spectrum of Cu. That is, *in-situ* ellipsometry in $scCO_2$ succeeded.

2) The observed Ψ and Δ spectra were not in agreement with those predicted by a single Cu layer model. The surface roughness of Cu was small and did not account for the disagreement.

3) Spectra fittings were carried out using a two-layer model consisting of an absorbing Cauchy dielectric on continuous Cu. It was found that a 15–50 nm-thick layer having a high refractive index is present on Cu. The complex refractive indices of this layer were determined at $(1.5–2) + (0.2–0.3)i$. This layer is the precursor layer condensed on the surface.

4) The condensed layer started to develop immediately after the precursor supply, and Cu started to grow afterwards. The thickness of the condensed layer was almost constant during Cu growth. Either precursor condensation or Cu growth starts earlier on Ru than on TiN.

5) Presence of the condensed layer is consistent with the hypotheses made by past researchers. In this study, we confirmed its presence. Multilayer adsorption and supersaturation–precipitation were discussed as possible formation mechanisms, and our experiments showed both characteristics.

Appendix: Procedure of Window Calibration

The windows of the optical cell affect the ellipsometric measurements due to the birefringence (photoelastic) effects. The calibration procedure used in this work is described here.

The polarization of the rotating polarizer ellipsometer we used in this work is mathematically described as

$$\boldsymbol{L}_{\text{out}} = \boldsymbol{A}\boldsymbol{R}(A)\boldsymbol{S}\boldsymbol{R}(-P)\boldsymbol{P}\boldsymbol{L}_{\text{in}} \tag{A·1}$$

where $\boldsymbol{L}_{\text{out}}$ is a Jones vector of the light sensed by a detector, $\boldsymbol{L}_{\text{in}}$, is that of a incident light, and $\boldsymbol{A}$, $\boldsymbol{S}$, $\boldsymbol{P}$, and $\boldsymbol{R}$(X) are Jones matrices of the analyzer, specimen, polarizer and the light axis rotation of an optical element X, respectively.

When an optical element is present between the specimen and the polarizer and between the specimen and the analyzer, eq. (A·1) becomes

$$\boldsymbol{L}_{\text{out}} = \boldsymbol{A}\boldsymbol{R}(A)\mathbf{J}\boldsymbol{S}\mathbf{J}\boldsymbol{R}(-P)\boldsymbol{P}\boldsymbol{L}_{\text{in}}. \tag{A·2}$$

In above equation, $\mathbf{J}$ is the Jones matrix of the element, which is expressed by[58]

$$\mathbf{J} = \begin{vmatrix} J_{\text{pp}} & J_{\text{sp}} \\ J_{\text{ps}} & 1 \end{vmatrix}, \tag{A·3}$$

$$\begin{aligned} J_{\text{pp}} &= \tan\Psi_{\text{pp}}\exp(i\Delta_{\text{pp}}), \\ J_{\text{sp}} &= \tan\Psi_{\text{sp}}\exp(i\Delta_{\text{sp}}), \\ J_{\text{ps}} &= \tan\Psi_{\text{ps}}\exp(i\Delta_{\text{ps}}), \end{aligned} \tag{A·4}$$

where Ψ and Δ are the birefringence parameters and the subscripts have appropriately-defined meanings. By substituting eqs. (A·3) and (A·4) to eq. (A·2), the components of $\boldsymbol{L}_{\text{out}}$ (electric field strength, E_{a} and E_{b}) are obtained as

$$\begin{aligned} E_{\text{a}} &= Q\cos A + Z\sin A, \\ E_{\text{b}} &= 0, \end{aligned} \tag{A·5}$$

where

$$\begin{aligned} Q &= J_{\text{pp}}S_1X + J_{\text{sp}}S_2Y, \\ Z &= J_{\text{ps}}S_1X + S_2Y, \\ X &= J_{\text{pp}}\cos P + J_{\text{sp}}\sin P, \\ Y &= J_{\text{ps}}\cos P + \sin P, \\ S_1 &= \sin\Psi_{\text{s}}\exp(i\Delta_{\text{s}}), \\ S_2 &= \cos\Psi_{\text{s}}, \end{aligned}$$

and Ψ_{s} and Δ_{s} are the ellipsometric parameters of the specimen.

The intensity of light is the square of the electric field amplitude, and is expressed as a function of the azimuth angle of the analyzer, A,

$$I = I_0(1 + \alpha\cos 2A + \beta\sin 2A), \tag{A·6}$$

where I_0 is a constant proportional to the intensity of the incident light and α and β are given by the below equations, respectively:

$$\alpha = \frac{|Q|^2 - |Z|^2}{|Q|^2 + |Z|^2},$$

$$\beta = \frac{(Q\bar{Z} + Z\bar{Q})}{|Q|^2 + |Z|^2}.$$

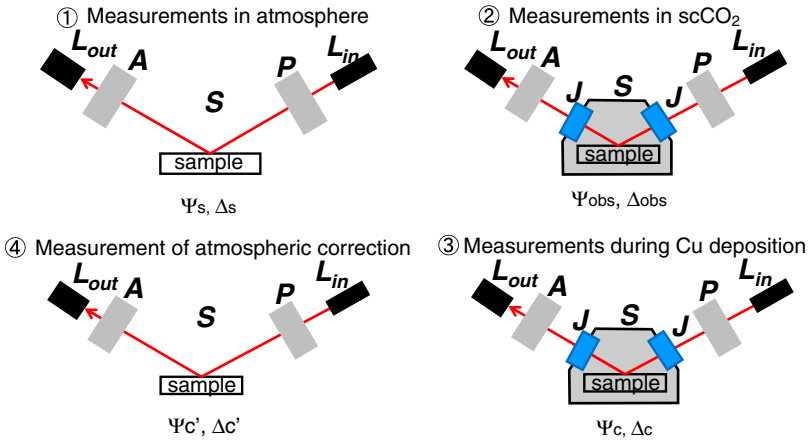

Fig. A·1. (Color online) Procedure of window correction.

Setting A to the angle of an actual ellipsometer, we obtain the following parameters of the light that pass the optical elements,

$$\tan \Psi_{\text{obs}} = \sqrt{\left(\frac{1+\alpha}{1-\alpha}\right)} \tan P,$$
$$\cos \Delta_{\text{obs}} = \frac{\beta}{\sqrt{1-\alpha^2}},$$

which are values of the specimen we observe. In our case, the windows and CO_2 environment correspond to the abovementioned optical element.

We get Ψ_s and Δ_s from a usual ellipsometric measurement carried out in the atmosphere before a deposition experiment. In principle, the 6 parameters in eq. (A·4) can be determined from the set of Ψ_s, Δ_s, Ψ_{obs}, and Δ_{obs}.

Equations (A·3) and (A·4) are general forms that take into account the anisotropy of the windows. We used amorphous glass windows, and the anisotropic effects are supposed to be negligible, i.e., J_{ps} and J_{sp} can be set to 0. As such, we have only J_{pp} as an unknown parameter. By redefining Ψ_{pp} and Δ_{pp} as the parameters of Ψ_w and Δ_w, where the subscript w indicates window, we obtain[59)]

$$(\tan \Psi_w)^2 = \frac{\tan \Psi_{\text{obs}}}{\tan \Psi_s}, \quad \text{(A·7)}$$
$$\Delta_w = \frac{\Delta_s - \Delta_{\text{obs}}}{2}. \quad \text{(A·8)}$$

The calibration procedure is illustrated in Fig. A·1. Ψ_s and Δ_s of a specimen are obtained in the atmosphere before deposition (Fig. A·1①). The same specimen was measured in $scCO_2$ and we obtained Ψ_{obs} and Δ_{obs} (Fig. A·1②). From eqs. (A·7) and (A·8), the window parameters Ψ_w and Δ_w of this particular experiment were obtained.

During the deposition experiment, the observed Ψ and Δ change due to Cu formation, for instance. Let us denote these parameters Ψ_C and Δ_C (Fig. A·1③). By substituting Ψ_C, Δ_C, Ψ_w, and Δ_w into eqs. (A·7) and (A·8), we obtain the calibrated ellpsometric parameters $\Psi_{C'}$ and $\Delta_{C'}$:

$$\Psi_{C'} = \tan^{-1} \frac{\tan \Psi_C}{(\tan \Psi_w)^2},$$
$$\Delta_{C'} = \Delta_C + 2\Delta_w. \quad \text{(A·9)}$$

1) R. Span and W. Wagner: J. Phys. Chem. Ref. Data **25** (1996) 1509.
2) O. A. Louchev, V. K. Popov, and E. N. Antonov: J. Cryst. Growth **155** (1995) 276.
3) J. M. Blackburn, D. P. Long, and A. Cabañas: Science **294** (2001) 141.
4) E. Kondoh and H. Kato: Microelectron. Eng. **64** (2002) 495.
5) D. P. Long, J. M. Blackburn, and J. J. Watkins: Adv. Mater. **12** (2002) 913.
6) X.-R. Ye, Y. Lin, C. Wang, M. H. Engelhard, Y. Wang, and C. M. Wai: J. Mater. Chem. **14** (2004) 908.
7) Y. Zhang, D. Kang, C. Saquing, M. Aindow, and C. Erkey: Ind. Eng. Chem. Res. **44** (2005) 4161.
8) E. Kondoh: Jpn. J. Appl. Phys. **44** (2005) 5799.
9) A. O'Neil and J. J. Watkins: Chem. Mater. **18** (2006) 5652.
10) B. Zhao, T. Momose, and Y. Shimogaki: Jpn. J. Appl. Phys. **45** (2006) 1296.
11) K. S. Morley, P. C. Marr, P. B. Webb, A. R. Berry, F. J. Allison, G. Moldovan, P. D. Brown, and S. M. Howdle: J. Mater. Chem. **12** (2002) 1898.
12) A. Cabañas, X. Shan, and J. J. Watkins: Chem. Mater. **15** (2003) 2910.
13) Y. Fukushima and H. Wakayama: J. Phys. Chem. B **103** (1999) 3062.
14) N. E. Fernandes, S. M. Fisher, J. C. Poshusta, D. G. Vlachos, M. Tsapatsis, and J. J. Watkins: Chem. Mater. **13** (2001) 2023.
15) E. Kondoh: Jpn. J. Appl. Phys. **43** (2004) 3928.
16) T. Momose, M. Sugiyama, E. Kondoh, and Y. Shimogaki: Appl. Phys. Express **1** (2008) 097002.
17) E. Kondoh, M. Matsubara, K. Tamai, and Y. Shimogaki: Jpn. J. Appl. Phys. **49** (2010) 05FA07.
18) R. Garriga, V. Pessy, F. Weill, B. Chevalier, J. Etourneau, and F. Cansell: J. Supercrit. Fluids **20** (2001) 55.
19) H. Sato, Y. Inada, T. Nagamura, and S. Funahashi: J. Supercrit. Fluids **21** (2001) 71.
20) M. Bremholm, H. Jensen, S. Brummerstedt Iversen, and B. Brummerstedt Iversen: J. Supercrit. Fluids **44** (2008) 385.
21) S. Dowy, A. Braeuer, K. Reinhold-Lopez, and A. Leipertz: J. Supercrit. Fluids **55** (2010) 282.
22) T. Momose, M. Sugiyama, and Y. Shimogaki: Jpn. J. Appl. Phys. **47** (2008) 885.
23) N. M. Felix, A. De Silva, C. M. Y. Luk, and C. K. Ober: J. Mater. Chem. **17** (2007) 4598.
24) E. Kondoh and S. Aruga: Microelectron. Eng. **88** (2011) 623.
25) M. Matsubara, M. Hirose, K. Tamai, Y. Shimogaki, and E. Kondoh: J. Electrochem. Soc. **156** (2009) H443.
26) E. Kondoh: U.S. Patent 7651671 (2010).
27) SOPRA n&k database.
28) H. Akimichi: Surf. Sci. **271** (1992) 184.
29) T. Kawagoe and T. Mizoguchi: Jpn. J. Appl. Phys. **32** (1993) 935.
30) From further model analyses, the formation of a 1–2-nm-thick CuO layer, or surface oxidation, accounts for the differences in the Ψ and Δ between bulk Cu and our films measured after deposition.
31) H. G. Tompkins: *A User's Guide to Ellipsometry* (Academic Press, San Diego, CA, 1993) p. 11.
32) It should be noted that the thicknesses shown here are not exactly same as those in Table II. In the data of Table II, sets of refractive index and thickness were obtained at each time. Contrarily, the thicknesses in Figs. 11 and 12 were obtained by assuming the refractive index of the X layer is constant during a run.

33) We carried out ellipsometric measurements on bulk $Cu(dibm)_2$ specimens and obtained a refractive index of approximately 1.4–1.5. Ellipsometry requires a very smooth surface for reliable measurements, and we were not able to prepare optically flat specimens. Therefore, this value is not very reliable. Even so, it is sure the accurate refractive index is higher than this value.
34) F. Karipcin, B. Dede, Y. Caglar, D. Hü, S. Ilican, M. Caglar, and Y. Şahin: Opt. Commun. **272** (2007) 131.
35) In fact, the X layer thickness decreased when the supply of $Cu(dibm)_2$ was terminated. This indicates the X layer formation is a reversible process and strongly supports our discussion that the X layer is a condensed precursor layer. We are planning to report the reversible nature in the near future.
36) E. Kondoh, K. Nagano, C. Yamamoto, and J. Yamanaka: Microelectron. Eng. **86** (2009) 902.
37) E. Kondoh, M. Hirose, E. Ukai, and K. Nagano: MRS Proc. **992** (2007) 992-D02-03.
38) E. Kondoh: Hyomen Gijutsu **61** (2010) 566 [in Japanese].
39) F. Kano, H. Uchida, and S. Koda: J. Supercrit. Fluids **50** (2009) 313.
40) J. Chrastil: J. Phys. Chem. **86** (1982) 3016.
41) R. M'Hamdi, J. F. Bocquet, K. Chhor, and C. Pommier: J. Supercrit. Fluids **5** (1992) 55.
42) M. Ohara, N. Fukui, M. Haruki, S. Kihara, and S. Takishima: presented at 76th Annu. Meet. Society of Chemical Engineers, Japan, 2011, D101.
43) Acetone was added in the system. The acetone may increase the solubility but is not supposed to affect the temperature dependence.
44) Y. Zong and J. J. Watkins: Chem. Mater. **17** (2005) 560.
45) E. Kondoh and J. Fukuda: J. Supercrit. Fluids **44** (2008) 466.
46) D.-H. Kim, R. H. Wentorf, and W. N. Gill: J. Electrochem. Soc. **140** (1993) 3267.
47) W. G. Lai, Y. Xie, and G. L. Griffin: J. Electrochem. Soc. **138** (1991) 3499.
48) N. S. Borgharkar and G. L. Griffin: J. Electrochem. Soc. **145** (1998) 347.
49) K. Ueno, Y. Shimada, S. Yomogida, S. Akahori, T. Yamamoto, T. Yamaguchi, Y. Aoki, A. Matsuyama, T. Yata, and H. Hashimoto: Jpn. J. Appl. Phys. **49** (2010) 05FA08.
50) I. Goswami and R. Laxman: Semicond. Int. **27** (2004) 49.
51) D. C. Perng, J. B. Yeh, and K. C. Hsu: Appl. Surf. Sci. **254** (2008) 6059.
52) Y. Takigawa, N. Tarumi, M. Shiohara, E. Soda, N. Oda, and S. Ogawa: Jpn. J. Appl. Phys. **50** (2011) 016503.
53) M. W. Lane, C. E. Murray, F. R. McFeely, P. M. Vereecken, and R. Rosenberg: Appl. Phy. Lett. **83** (2003) 2330.
54) O. Chyan, T. N. Arunagiri, and T. Ponnuswamy: J. Electrochem. Soc. **150** (2003) C347.
55) T. Waechtler, S.-F. Ding, L. Hofmann, R. Mothes, Q. Xie, S. Oswald, C. Detavernier, S. E. Schulz, X.-P. Qu, H. Lang, and T. Gessner: Microelectron. Eng. **88** (2011) 684.
56) J. Shin, H.-W. Kim, G. S. Hwang, and J. G. Ekerdt: Surf. Coatings Technol. **201** (2007) 9256.
57) H. Kim, Y. Kojima, H. Sato, N. Yoshii, S. Hosaka, and Y. Shimogaki: Jpn. J. Appl. Phys. **45** (2006) L233.
58) M. Schubert, B. Rheinlander, J. A. Woollam, B. Johs, and C. M. Herzinger: J. Opt. Soc. Am. A **13** (1996) 875.
59) This treatment is eventually identical to multiplying a complex coefficient to the ratio of complex reflectivities, however, is more rigorously derived here.